Biogenic Synthesis of ZnO Nanoparticles Mediated From *Borassus Flabellifer (Linn)*: Antioxidant, Antimicrobial Activity Against Clinical Pathogens, And Photocatalytic Degradation Activity With Molecular Modeling.

Dharman Kalaimurgan
Periyar University
Kandhasamy Lalitha
Periyar University
Kaliannan Durairaj
Periyar University
Palaniappan Sivasankar (sivasankar.ps@gmail.com)
Periyar University https://orcid.org/0000-0002-1930-7657
Sungkwon Park
Sejong University
Kannan Nithya
Periyar University
Muthugoundar Subramanian Shivakumar
Periyar University
Wenchao Liu
Zhanjiang Ocean University: Guangdong Ocean University
Balasubramanian Balamuralikrishnan
Sejong University
Srinivasan Venkatesan
Periyar University

Research Article

Keywords: Borassus flabellifer, Zinc-Oxide nanoparticles, Antimicrobial activity, In-silico docking, Photocatalytic

Posted Date: April 19th, 2021

DOI: https://doi.org/10.21203/rs.3.rs-224964/v1

Abstract

Borassus flabellifer leaf extract has been used for rapid biogenic-synthesis of Zinc-Oxide nanoparticles (ZnO-NPs) due to rich source of bioactive compounds. The synthesized ZnO-NPs were preliminarily confirmed by UV-Visible spectroscopy adsorption peak range at 365nm. The XRD (X-ray diffraction) confirm purity of ZnO-NPs that were crystalline in nature. The analysis of FT-IR (Fourier-transform infrared spectroscopy) confirm the presence of following functional group such as alcohol, phenols, carboxylic acids, primary amides, secondary amides, alkyl halide. FE-SEM analysis indicated that ZnO-NPs were in spherical shape, followed by EDX analysis which confirmed the presence of Zn-element. Antimicrobial effect of ZnO-NPs was investigated using different clinical pathogens like bacteria *Staphylococcus aureus, Bacillus subtilis, Escherichia coli*, *Klebsiella Pneumonia*, *Pseudomonas aeruginosa* and fungi *Aspergillus flavus*, *Candida albicans* and *Penicillium expansum* and which confirmed ZnO-NPs efficiency as an antimicrobial agent. Antioxidant activity were ascertained to used for several biomedical applications. The ZnO-NPs was efficiently degraded the environmental toxic dyes (methylene blue and crystal violet) under sunlight. In support of photolight-degradation, the study was progressed to understand the ZnO-dye interaction stability using molecular mechanism and it was showing efficient bonding features in the NPs environment. Overall, this investigation have great potential for being an effective and eco-friendly materials was used in environmental applications.

Highlights

- *B. flabellifer* leaf is used for synthesis of Zinc oxide nanoparticles (ZnO-NPs).
- The ZnO-NPs synthesized material were characterized by UV-Spectra, XRD, FE-SEM and EDX.
- *B. flabellifer* leaf extract and its derived Zn-NPs have been tested for their antibacterial, antifungal, antioxidant, photocatalytic activity.
- In backing of photocatalytic study, proceeded to *in-silico* docking analysis.
- This simple biological approaches are non-toxic, environmentally safe and cost efficient.

Introduction

Nanotechnology is one of the most fascinating ideas which is to develop particles with nano size for the use in various fields of science and technology such as increased surface area, catalytic efficiency, profuse reactive sites as well as high absorption rates (Dhand et al. 2015; Cittrarasu et al. 2019). There are several types of nanomaterials that have been used like nanocage, nanowire, quantum dot, nanocomposite and nanoparticles (Kalaimurugan et al. 2019). Green chemistry way for metallic and metallic oxide nanoparticle synthesis was especially intended to condense the ecological noxiousness or remove the conservational effluence. Zinc oxide (ZnO) shows a dynamic part in the day-to-day life of the 3rd uppermost universal making volume only after SiO2 and TiO2 among the safest metal to use and also has the confirmed biocompatibility summary that “generally recognized as safe” (GRAS) material to the human and animal system by the USFDA (21CFR182.8991) (Piccinno et al. 2012). Recent studies

have shown that inc oxide nanoparticles (ZnO-NPs) have potent toxicity to bacteria but exhibit minimal effects on human cells (Reddy et al. 2007). The ZnONPs are used in textiles for water treatment and sunscreen lotion, because it possess high photocatalytic degradation (Dhand et al. 2015). The disposals of dyes without any treatment will leads to serious threat to the environment and aquatic system. Further certain dyes like reactive dyes are recalcitrant, non-biodegradable, toxic and mutagenic (Dalvand et al. 2016). Therefore, there is a need for biological alternatives of producing ecofriendly NPs. The *Borassus flabellifer* (Linn) (Palmyra palm tree) belongs to *Arecaceae* family and is extensively available in Asian regions such as India, Bangladesh, Thailand, Srilanka, etc. The *B. flabellifer* is used widely for variety of purposes such as stimulant, anti-laprotic, diuretic and antiphlogistic. Studies have shown no biogreen syntheis of ZnO-NPs has been done using *B. flabellifer* leaf extract (BFLE). In this study, using BFLE as reduction agent we aimed at green synthesis of ZnO-NPs and characterized by UV-visible spectroscopy, X-ray diffractometer (XRD), Field Emission Scanning Electron Microscope (FE-SEM), Energy-dispersive X-ray spectroscopy (EDS). Further investigated their antibacterial, antifungal activity against representatives of clinical pathogenic microorganisms, antioxidant activity of radical scavenging activity and photocatalytic degradation of methylene blue and crystal violet dyes under sunlight along with in-silico molecular docking analysis to shed more light on the pharmaceutical and industrialized research findings.

Materials And Methods

2.1. Preparation of BFLE

The *B. flabellifer* plant leaves were collected (Salem, Tamil Nadu, India), air dried, powdered and then dissolved in 100 mL of distilled water. The aqueous part was separated using Whatmann no.1 filter paper after boiling at 60^{o}C for 15 min and stored in refrigerator. All the other chemicals used in this experiment were analytical grade reagents.

2.2. Synthesis and Characterization of ZnO-NPs

The ZnO-NPs were prepared by adding 80 mL of 1 mM aqueous $ZnSO_4$ into 20 mL BFLE to foram a reaction ixture with continious stirring at at 60ºC for 15 min. Once the ZnO-NPs production was completed, it wassubjected to centrifugation at 10,000 rpm for 20 min at 4°C, followed by several washes with nanopure water and ethanol. The obtained material was freeze-dried to make a powder. The freeze-dried powder was used for further characterization and photocatalytic study. Biosynthesis of ZnO-NPs were characterized using UV-Visible Spectrophotometer to determining the absorption peak. The XRD was measured at the voltage of 40.0 (kV) and the current supplied by 30.0 (kV) with the sample scanning range at 10,000–90,000 for the determination and evaluation of crystalline structure of ZnO conjugated with BFLE. The FT-IR analysis of plant leaf extract and ZnO-NPs was made to identify the presence of functional groups and chemical bonding. The 3-D image of a particle size, elemental composition analysis, surface characterization and magnification were analyzed using FE-SEM and EDS (Singh and Dutta 2020).

2.3. Antibacterial activity

The *B. flabellifer* ZnO-NPs were tested for their antibacterial activity against clinical pathogenic bacteria by Agar Well diffusion methods (Cittrarasu et al. 2019). To the Muller Hinton agar culture plate, five pathogenic bacteria *Staphylococcus aureus*, *Bacillus subtilis*, *Escherichia coli*, *Klebsiella pneumoniae*, *Pseudomonas aeruginosa* were swabbed separately and wells were punched. The ZnO-NPs dissolved in Dimethyl Sulfoxide (DMSO) were pipetted out at different concentrations (20, 40, 60, 80 and 100 µl/mL) in the appropriate wells and as a control antibiotic tetracycline was used. Petri-dishes were incubated at 37°C for 24 h and the zone of inhibition (mm) was recorded.

2.4. Antifungal activity

The antifungal activity of synthesized ZnO-NPs along with plant *B. flabellifer* leaf extracts against pathogenic fungus was followed by Jamdagni et al. (2018). To the potato dextrose agar culture plate, three fungus *Aspergillus flavous*, *Candida albicans* and *Pencillium expansum* were swabbed separately and wells were made using gel puncher. Different concentrations (20, 40, 60, 80 and 100 µl/mL) of samples were pipetted out in the appropriate wells and as a control fluconazolewere used. Petri-dishes were incubated at 25°C for 72 h and the zone inhibition (in mm) was measured and recorded .

2.5. Antioxidant activity

2.5.1. 2, 2-Diphenyl-1-Picrylhydrazyl assay (DPPH)

The DPPH activity was performed by the modified protocol described previously (Suresh et al. 2015). The constant free radicals of DPPH in oxidized form exist in purple color and the absorbance was measured at 520 nm. As a positive control ascorbic acid was used. The stock solution of ascorbic acid was made by adding 3 mg of ascorbic acid to the 15 mL of deionizer water. Further, different concentrations (20, 40, 60, 80, 100 µg/mL) were used to plot the standard graph. The scavenging activity of inhibition in percentage for each concentration was calculated using standard graph by the following formula,

DPPH Scavenging effect (%) = A_0-A_1/A_0*100 ----- (1)

Whereas, A_0- absorbance of control, A_1- absorbance of sample

2.6. Photocatalytic activity of ZnO-NPs

The photocatalytic activity of the ZnO-NPs was performed with methylene blue (30 mg/L), crystal violet (30 mg/L) dyes at neutral pH and ambient temperature. The method was analyzed as follows; 0.10 g of synthesized products were dispensed in 10 mL of different dye solution in a container provided with water flow ability. To find the homogeneous solution, the above suspension was continually stirred in the absence of radiation for about 30 min. This is performed to achieve adsorption and desorption equilibrium. The sun light was used as light source. In a typical photocatalytic activity process, 20 mg sample was added to 10 mL of dye solution and the adsorption spectrum of the solution was monitored using UV- visible spectrophotometer (Cittrarasu et al. 2019).

2.7. Molecular configuration of ZnO with dyes.

Structure of methylene blue (CID_6099) and crystal violet (CID_11057) was downloaded from NCBI-PubChem. The 2D-structure was optimized using Chem sketch individually. Both the stuctures were maintained for Universal force field spatial configuration. The ZnO-NPs was drawn and prepared for penta NP layer. The complex of ZnO and NPs was subjected to simulate under vacuum for 100 ns using Gromacs Sunghwan et al. 2016; Duffy et al. 2000). The resultant structure was plotted based on root mean square deviation value of the complex interactions.

2.8. Statistical analysis

Statistical comparisons were done using Student's t test $p < 0.05$ was considered as a significant value. The inhibition zone of inhibition was estimated in diameter (mm) using two-way variance analysis (ANOVA) and expressed as Mean ± Standard Deviation (GraphPad Prism version 6.0).

Results And Discussion

In the present study, BFLE with $ZnSO_4$ solution showed colour change to dark brown, that confirms the presence of ZnO-NPs. Similar study on synthesized ZnNPs using *A. calamus* aqueous extract exhibit colour change from transparent to reddish dark brown (Duffyet al. 2000; Ibrahim et al. 2017; Suresh et al. 2015 Abdullahi and Harun 2017). Also, ZnO-NPs synthesis used two kinds of chemical agents (i) zinc sulfate acts as precursor and (ii) phenolic and flavonoids components of BFLE act as reduction agents. In this study, ZnO-NPs exhibit strong peak from the spectra at the range of 365 nm under UV-visible spectrophotometer (Fig. 1a). Whereas, previous study of synthesized ZnO-NPs using *Olea europea* leaf extract showed absorption peak at 374 nm (Awwad et al. 2014). The XRD-analysis revelas the phase of ZnO-NPs using aqueous BFLE. The synthesized ZnO-NPs showed three strongest peaks of lattice plane at (100), (101) and (102) (Fig. 1b). This strongly confirms the ZnO-NPs are in spherical shape. Study on synthesized ZnO-NPs using *J. curcas* latex showed the XRD lattice plane at (111), (200), (220) and (311) and this corroborate the crystalline structure (Safawo et al. 2018) .

The FT-IR spectra analysis and functional groups present in synthesized ZnO-NPs was observed with wavelength related to the vibration assignments, as well as corresponds to visible intensity. The FT-IR result shows that, the medium peak values at 3418.67, 2926.85, 1625.88, 1384.58, 1317.28, 916.99, 563.71 and 431.39 cm^{-1} of alcohol, phenols, carboxylic acids, primary amides, secondary amides, alkyl halide respectively, These are the functional groups are present in the biosynthesis of nanoparticles and plant leaf extract (Fig. 2, Table 1, 2). The surface functional groups and capping of synthesized ZnO-NPs were identified under FT-IR spectroscopy. The FT-IR analysis of previous study reported that the band at 3200–3500 cm^{-1}, 1617 cm^{-1}, 890 cm^{-1}, 1534 cm^{-1} and 1458 cm^{-1} revealed O-H stretching, bending vibration of H_2O molecules, one transmission band due to C-O, asymmetry and symmetry vibration of –COOH group and its' confirms the presence of ZnO-NPs. In the current study, the functional groups at 3418.67 cm^{-1}, 2926.85 cm^{-1}, 1625.88 cm^{-1}, 1384.58 cm^{-1}, 1317.28 cm^{-1}, 916.99 cm^{-1}, 563.71 cm^{-1} and 431.39 cm^{-1} were observed. All these bands clearly indicates that, the functional groups were involved in the formation of ZnO-NPs (Kalaimurugan et al. 2019).

Table 1
The FT-IR functional group's analysis for *B. flabellifer* leaf extract.

Vibrational assignment	Observed wavenumber (cm^{-1})	Functional group	Visible intensity
O-H stretching	3911.73	Alcohol	Small peak
O-H stretching	3879.35	Alcohol	Small peak
O-H stretching	3208.64	Alcohol	Small medium peak
N-H stretching	2923.26	Amine	Small sharp peak
N-H stretching	2854.73	Amine	Small sharp peak
C≡C stretching	2209.32	Alkyne	Small peak
C = O stretching	1734.48	Aldehyde	Small peak
C-H bending	1452.88	Alkane	Small peak
C-H bending	1398.04	Aldehyde	Small sharp peak
O–H bending	922.50	Carboxylic acids	Small peak
C–Br stretch	600.53	Alkyl halides	Sharp peak
C–Br stretch	552.45	Alkyl halides	Small peak

Table 2
The FT-IR functional group's analysis for *B. flabellifer* leaf mediated ZnNPs.

Vibrational assignment	Observed wavenumber (cm^{-1})	Functional group	Visible intensity
O–H stretch	3418.64	Alcohol and phenols	Small medium peak
O–H stretch	2926.85	Carboxylic acids	Small medium peak
C-H stretch	2854.56	Aldehydes	Small medium peak
NH_2	1625.88	Primary amids	Wide peak
NO_2	1384.58	Aliphatic nitro	Very sharp peak
C–O stretch	1317.28	Anhydrides	Very sharp peak
C–O–H stretch	916.59	Carboxylic acids	Medium peak
N–H wagging	782.14	Secondary amide	Very sharp peak
C-Cl stretch	563.71	Alkyl halide	Wide peak
C-I stretch	431.39	Alkyl halide	Small sharp peak

The FE-SEM analysis was performed to image (at 1-200 µm magnifications) the shape and size of BFLE-capped ZnO-NPs (Fig. 3a,b) and this clearly determines the ZnO-NPs are spherical in shape with 50 nm in diameter (Fig. 3c,d). The purity was further determined with EDX analysis. Previous study on ZnO-NPs using *Z. clinopodioides* leaves showed exhibit spherical shape with particle size ranges from 5–40 nm. In recent study, the synthesized ZnO-NPs showed strong silver signal along with other molecules like weak oxygen, carbon and aluminium (Suresh et al. 2015). Likewise, in our present study, through the EDX-analysis the presence of higher concentration of Zn were determined (Kalaimurugan et al. 2019).

The DPPH assay provides an easy and fast antioxidant activity by total estimation method. The colour changes from purple to yellow after reduction, which can be quantified at 519 nm due to its reduced absorbance. As the concentration increased (20 µg/mL–18.47 %; 40 µg/mL – 34.66 %; 60 µg/mL – 49.01 %; 80 µg/mL – 61.03 % and 100 µg/mL – 73.27 %), free radical scavenging activity of ZnO-NPs on DPPH was observed (Fig. 4). The antibacterial activity of biosynthesized ZnO-NPs was investigated at different concentrations (20, 40, 60, 80, 100 µg/mL) along with the positive control, tetracycline against clinical pathogen *S. aureus*, *B. subtilis*, *E. coli*, *K. pneumonia* and *P. aeruginosa* (Fig. 5a and Table 3). We also cross checked the plant extract alone for antibacterial activity and no zone of inhibition was observed. Only synthesized nanoparticles combined with plant extract (secondary metabolites) showed better result and this may be due to the sensitivity to zone of inhibition. Antifungal activity of biosynthesized ZnO-NPs was investigated at various concentrations (20, 40, 60, 80, 100 µg/mL) against three fugus *A. flavus, C.*

albicans and *P. expansum*. The antifungal activity of ZnO-NPs is shown in Fig. 5b and the zone inhibition is shown in Table 4. The fungus *A. flavus* had a medium sensitivity to 100 µg/mL, other two fungal species had a strong sensitivity to 100 µg/mL ZnO-NPs. Figure 6 showed that the schematic reason for mechanism of microbes cell damage by ZnO-NPs.

Table 3
Antibacterial activity of synthesized ZnNPs against pathogenic bacteria

	Zone of inhibition (mm) with Mean ± SD				
Conc. (µl/mL)	*Staphylococcus aureus*	*Bacillus subtilis*	*Escherichia coli*	*Klebsiella pneumoniae*	*Pseudomonas aeruginosa*
Control	14.83 ± 0.2	15.66 ± 0.4	16.66 ± 0.4	17.66 ± 0.4	18.66 ± 0.4
20	5.66 ± 0.4	7.16 ± 0.2	6.83 ± 0.6	7.33 ± 0.4	7.50 ± 0.4
40	7.66 ± 0.4	8.66 ± 0.4	7.66 ± 0.4	9.66 ± 0.4	9.66 ± 0.4
60	9.50 ± 0.4	8.66 ± 0.4	8.66 ± 0.4	9.50 ± 0.4	11.66 ± 0.4
80	12.66 ± 0.4	11.83 ± 0.2	12.0 ± 0.8	13.66 ± 0.4	14.66 ± 0.4
100	15.66 ± 0.4	13.0 ± 0.8	15.83 ± 0.2	16.50 ± 0.4	17.83 ± 0.2

Table 4
Antifungal activity test of ZnNPs against some pathogenic fungi strains

	Zone of inhibition (mm) with Mean ± SD		
Conc. (µl/mL)	*Aspergillus flavus*	*Candida albicans*	*Penicillium expansum*
Control	12.66 ± 0.4	14.66 ± 0.4	15.66 ± 0.4
20	3.66 ± 0.4	4.5 ± 0.4	5.66 ± 0.4
40	5.83 ± 0.2	6.66 ± 0.4	7.83 ± 0.2
60	7.83 ± 0.2	8.66 ± 0.4	8.66 ± 0.4
80	9.66 ± 0.4	11.5 ± 0.4	12.66 ± 0.4
100	12.66 ± 0.4	13.66 ± 0.4	14.83 ± 0.2

An agent's antibacterial activity is due primarily to two mechanisms, which involve chemically interfering with the synthesis or function of essential components of bacteria and circumventing traditional mechanisms of antibacterial resistance (Mirza et al. 2019; Saravanan et al. 2018). Elumalai et al. (2010) reported that the antifungal activity of synthesized nanoparticles using *E. hirta* against 7 clinically isolated funguses (*C. albicans*, *C. kefyr*, *A. niger*, *C. tropicalis*, *C. krusei*, *A. flavus* and *A.fumigatus*) were tested. Among them *C. albicans*, *C. kefyr*, *A. niger* exhibit higher zone of inhibition at 50 µg/mL. We have

sucessfully demostrated that strong effects of antifungal activity of ZnO-NPs on fungus strains (*C. albicans, A. niger* and *P. expansum*). There was an increase in the inhibition zone while ZnO-NPS increased. A probable inhibitory mechanism can be clarified by oxygen species released on the surface of ZnO, which binding the bacterial surfaces and kills the bacteria through electro-static forces. However, it can be assumed that the free Zn^{2+} partially contributes the antimicrobial effect through the mechanical contact between the bacteria and ZnO rods surface. Likely, ZnO-NPs acted as needles that penetrating the bacterial cell wall which associates with the greater antimicrobial efficacy of the nano size over their micro counterparts (Saravanan et al. 2018 ; Elumalai et al. 2010). Previous study reported that the antibacterial activity against *S. aureus B. subtilis*, *E. coli*, *K. pneumonia P. aeruginosa* and *C. albicans*, *A. niger* and *P. expansum* were tested and higher zone of inhibition observed as well as antifungal activity against *C. albicans* by using plant extract derived ZnO-NPs Mahdavi et al. 2019; Xie et al. 2011). The ZnO-NPs have prominent antimicrobial activities (< 100 nm) due to large surface volume ratio facilitate the better dissolution and penetration of the bacteria (Piccinno et al. 2012). Thus, the results of our experiment revealed the excellent antifungal and antibacterial effects of ZnO-NPs against all of the tested bacteria and fungi.

The photocatalytic operation is strongly dependent on the crystallographic structure, morphology and size of the metal oxide NPs and colour degradation with the aid of sunlight. [Cittrarasu et al. 2019; Duffy et al. 2000). The dye degradation mechanisms was shematically presenterd in Fig. 7. Increased concentrations of methylene blue, crystal violet were tested with fixed amount of ZnO-NPs. The effect of dye concentration on ZnO-NPs photocatalytic function was accessed (Fig. 8). Our present study the maximum absorption rate was observed at 350 nm for methylene blue and 635 nm for crystal violet. After 1 hour, the dye slowly decreases with increased visible light exposure time and this shows the plot between time and dye concentration at different times. The complex of NPs and dyes were examined using molecular mechanics to understand the behviour of the interacted complex. The ZnO-NPs layers were maintained to have 120º for each Zn and Oxide group interactions, mean while the position of individual NPs were also properly placed the dynamic environment. All atoms in the systems are intentionaly maintained to have non-bnonded interaction types. The ZnO and one molecule of methylene blue and crystal violet was subjected to interact and simulated in the vacuum environment for 100 ns (Fig. 9a,b). The resultant structure was proportionally stable in the proposed environment. The trajectory of the each ZnO-NPs layer placed was propogated the equal environmental projections. It exhibits the energy containment to carry the dye with in the layer was stable and steady in the system. The RMSD shows (Fig. 9c,d) equal distribution of the distance deviation from each native structure.

Conclusion

In this study BFLE-conjugated ZnO-NPs were synthesized and characterized. The results showed that the average absorption was obtained at 365 nm and the scale of approximately 10–200 nm by FE-SEM, EDAX analysis in atoms element composition presented in synthesis of NPs conformed bind to the Zn present. The XRD analysis indicated the peak in crystalline nature. The biosynthesized ZnO-NPs were

verified to have excellent antibacterial and antifungal activity against clinical pathogens with potential antioxidant capacity. Further, methylene blue and crystal violet dyes were effectively degraded in the presence of ZnO-NPs. *In silico* analysis support the functional features of ZnO-dye interactions in the various environment under photocatalytic activity. Therefore, eco-friendly BFLE-mediated ZnO-NPs opens a new-fangled path of methods for production and could be potentially utilized for biomedical and industrial applications.

Declarations

Declaration of competing interest

The authors declare that they have no competing interests.

Acknowledgements

The authors are thankful to Periyar University, India for providing the necessary facility and also grateful to the Sejong University, Republic of Korea for their support of instrumental analysis facility.

References

Abdullahi T, Harun Z, Othman MHD (2017) A review on sustainable synthesis of zeolite from kaolinite resources via hydrothermal process. Advan Pow Techno 28:1827–1840

Awwad M, Borhan A, Ahmad L (2014) Green synthesis, characterization and optical properties of zinc oxide nanosheets using *Oleaeuropea* leaf extract. Adv Mat Lett 5:520–524)

Cittrarasu V, Balasubramanian B, Kaliannan D, Maluventhan V, Kaul T, Liu WC, Arumugam M (2019) Biological mediated Ag nanoparticles from Barlerialongiflora for antimicrobial activity and photocatalytic degradation using methylene blue. Artif Cells Nanomedicin Biotechnol 47:2424–2430

Dalvand A, Nabizadeh R, Ganjali MR, Khoobi M, Nazmara S, Mahvi AH (2016) Modeling of Reactive Blue 19 azo dye removal from colored textile wastewater using L-arginine-functionalized Fe3O4 nanoparticles: Optimization, reusability, kinetic and equilibrium studies. J Magn Magne Mater 404:179–189

Dhand C, Dwivedi N, Loh XJ, Ying ANJ, Verma NK, RW (2015) Beuerman, Ramakrishna. Methods and strategies for the synthesis of diverse nanoparticles and their applications: a comprehensive overview. Rsc Advances Rsc Advances 5:105003–105037

Duffy EM, Jorgensen WL (2000) Prediction of properties from simulations: free energies of salvation in Hexa decane, octanol, and water. J Am Chem 122:2878–2888

Elumalai EK, Prasad TNVKV, Kambala V, Nagajyothi PC, David E (2010) Green synthesis of silver nanoparticle using Euphorbia hirta L and their antifungal activities. Arch Appl Sci Res 2:76–81

Ibrahim MB, Abdullahi SH (2017) Green synthesis of zinc nanoparticles using *Ipomoea asarifolia* leaves extract and its adsorption properties for the removal of dyes. J Pure Appl Sci 10:7–14

Jamdagni P, Khatri P, Rana JS (2018) Green synthesis of zinc oxide nanoparticles using flower extract of Nyctanthesarbor-tristis and their antifungal activity. J Kin Sau Univer Sci 30:168–175

Kalaimurugan D, Vivekanandhan P, Sivasankar P, Durairaj K, Senthilkumar P, Shivakumar MS, Venkatesan S (2019) Larvicidal activity of silver nanoparticles synthesized by Pseudomonas fluorescens YPS3 isolated from the Eastern Ghats of India. J Clus Sci 30:225–233

Kalaimurugan D, Sivasankar P, Lavanya K, Shivakumar MS, Venkatesan S (2019) Antibacterial and larvicidal activity of Fusarium proliferatum (YNS2) whole cell biomass mediated copper nanoparticles. J Clu Sci 30:1071–1080

Mahdavi B, Saneei S, Qorbani M, Zhaleh M, Zangeneh A, Zangeneh MM, Ghaneialvar H (2019) Ziziphora clinopodioides Lam leaves aqueous extract mediated synthesis of zinc nanoparticles and their antibacterial, antifungal, cytotoxicity, antioxidant, and cutaneous wound healing properties under in vitro and in vivo conditions. Appl Organomet Chemi 33:5164

Mirza AU, Kareem A, Nami SA, Bhat SA, Mohammad A, Nishat N (2019) Malus pumila and Juglen regia plant species mediated zinc oxide nanoparticles: Synthesis, spectral characterization, antioxidant and antibacterial studies. Microb Pathog 129:233–241

Piccinno F, Gottschalk F, Seeger S, Nowack B (2012) Industrial production quantities and uses of ten engineered nanomaterials in Europe and the world. J Nanoparti Resear 14:1–11

Reddy KM, Feris K, Bell J, Wingett DG, Hanley C, Punnoose A (2007) Selective toxicity of zinc oxide nanoparticles to prokaryotic and eukaryotic systems, Appl. Phys. Lett. 90

Safawo T, Sandeep BV, Pola S, Tadesse A (2018) Synthesis and characterization of zinc oxide nanoparticles using tuber extract of anchote (Cocciniaabyssinica (Lam.) Cong.) for antimicrobial and antioxidant activity assessment. Open Nano 3:56–63

Saravanan M, Gopinath V, Chaurasia MK, Syed A, Ameen F, Purushothaman N (2018) Green synthesis of anisotropic zinc oxide nanoparticles with antibacterial and cytofriendly properties. Microb Pathog 115:57–63

Singh A, Dutta PK (2020) Green synthesis, characterization and biological evaluation of chitin glucan based zinc oxide nanoparticles and its curcumin conjugation. Interna J biologi Macromole 156:514–521

Sunghwan K, Paul AT, Evan EB, Chen J, Gang F (2016) PubChem Substance and Compound databases. Nucleic Acids Res 44:D1202–D1213

Suresh D, Nethravathi PC, Udayabhanu H, Rajanaika H, NagabhushanaSC, Sharma C (2015) Green synthesis of multifunctional zinc oxide (ZnO) nanoparticles using Cassia fistula plantextract and their photodegradative, antioxidant and antibacterial activities. Mater Sci Semicond Process 31:446–454

Xie YP, He YP, Irwin PL, JinT, Shi XM (2011) Antibacterial activity and mechanism of action of zinc oxide nanoparticles against Campylobacter jejuni. Appl Environ Microbiol 77(7):2325–2331

Figures

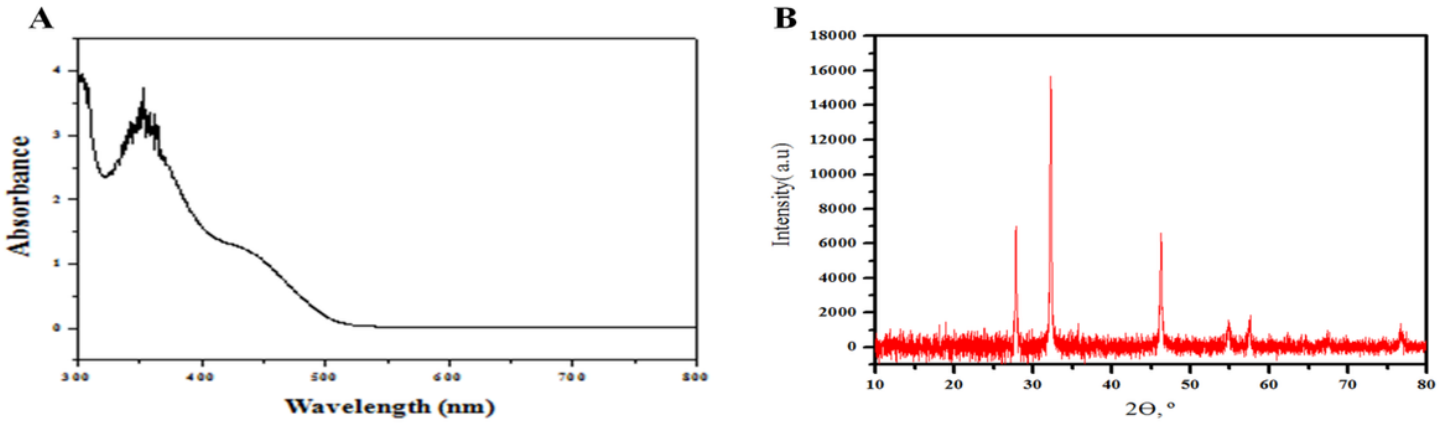

Figure 1

A) UV-vis spectrum of BFLE-mediated ZnO-NPs B) XRD pattern of synthesized ZnO-NPs shows 3 strongest peak values, which is corresponding to the intense counts.

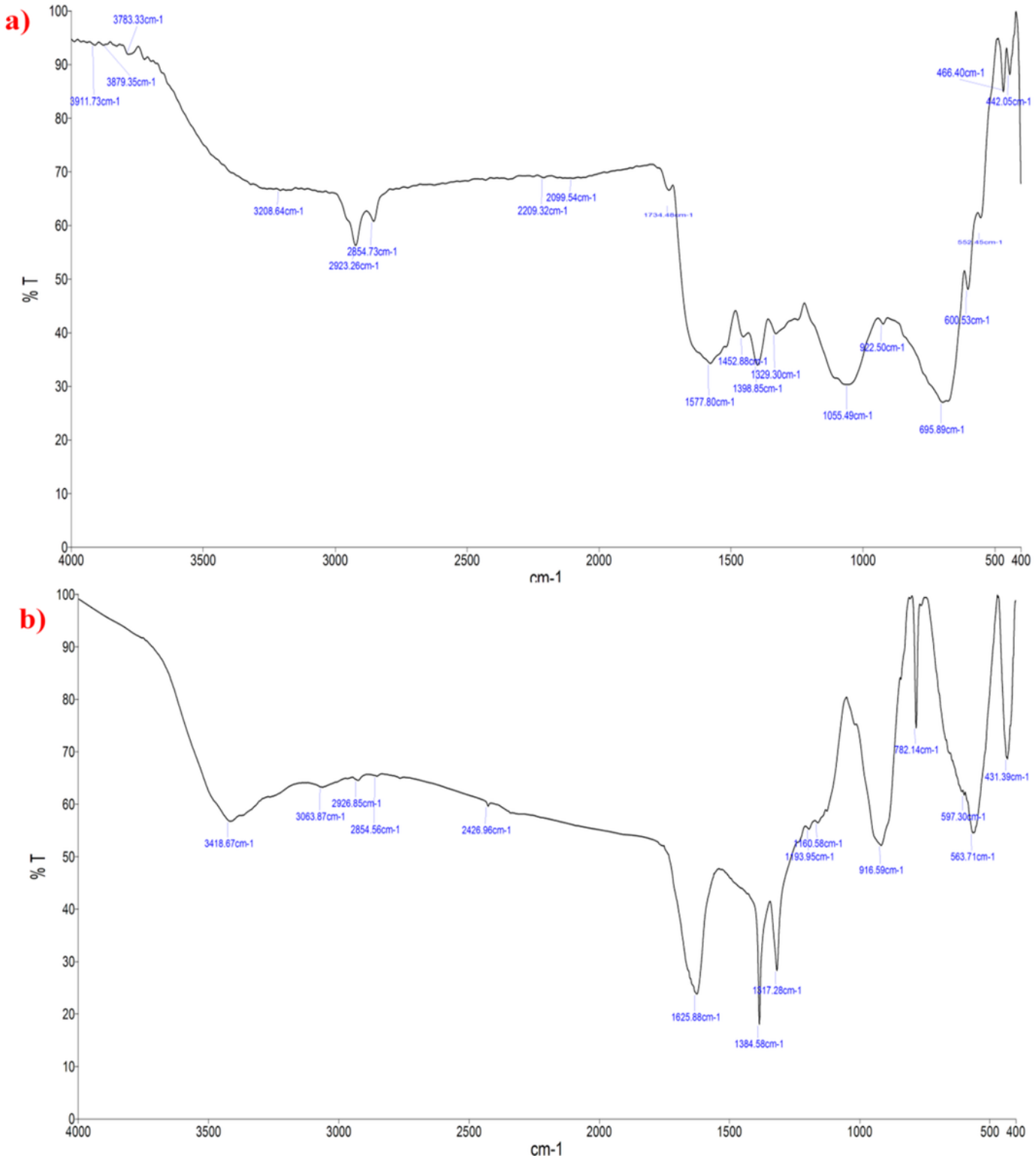

Figure 2

FT-IR spectrum analysis in ZnNPs a) plant extracts b) ZnNPs with plant extract.

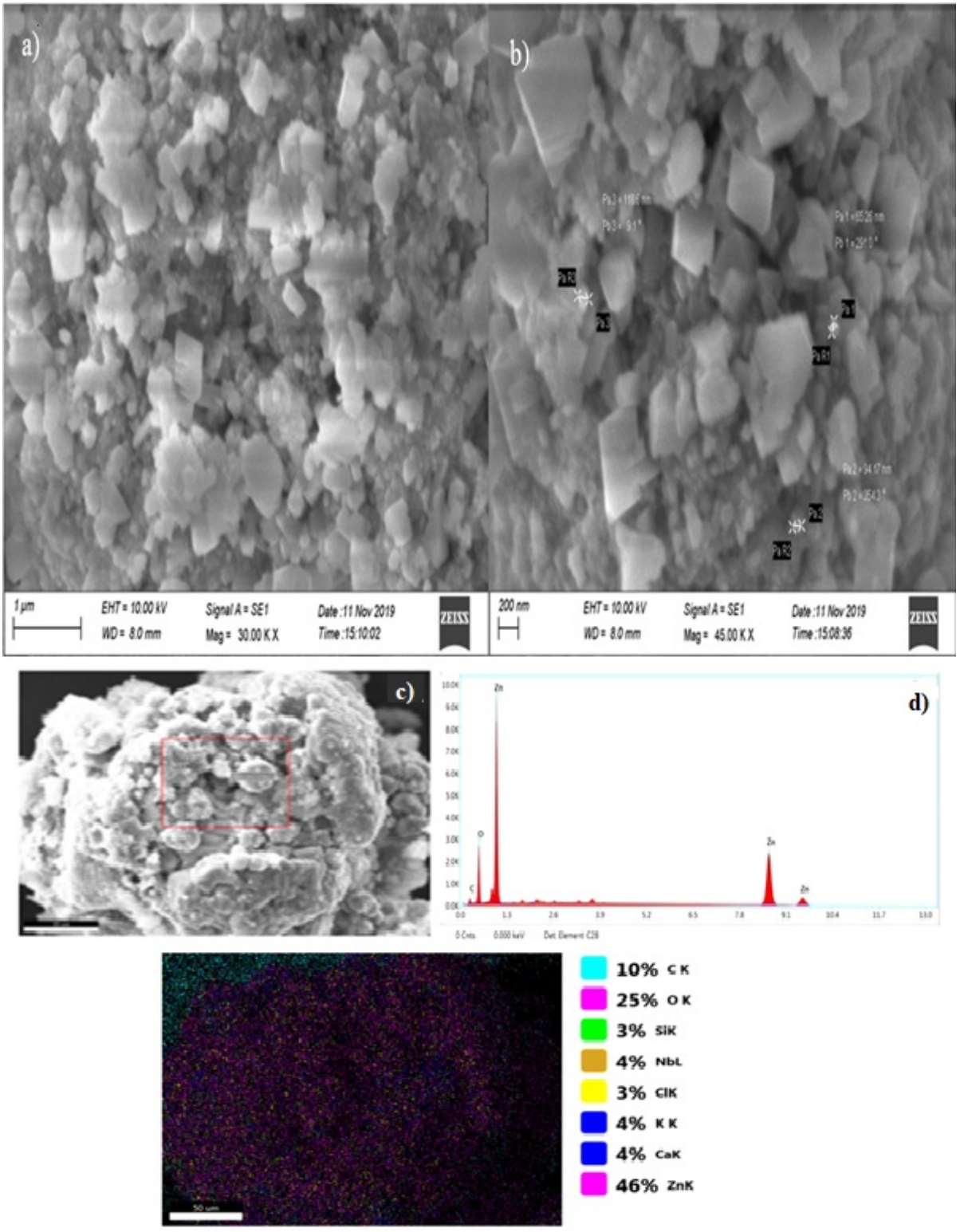

Figure 3

High Resolution Scanning Electron Microscopic (HRSEM) images of ZnO-NPs in different magnification ranges (a) 1 µm (b) 200 nm with EDX analysis (c, d) of BFLE in ZnO-NPs.

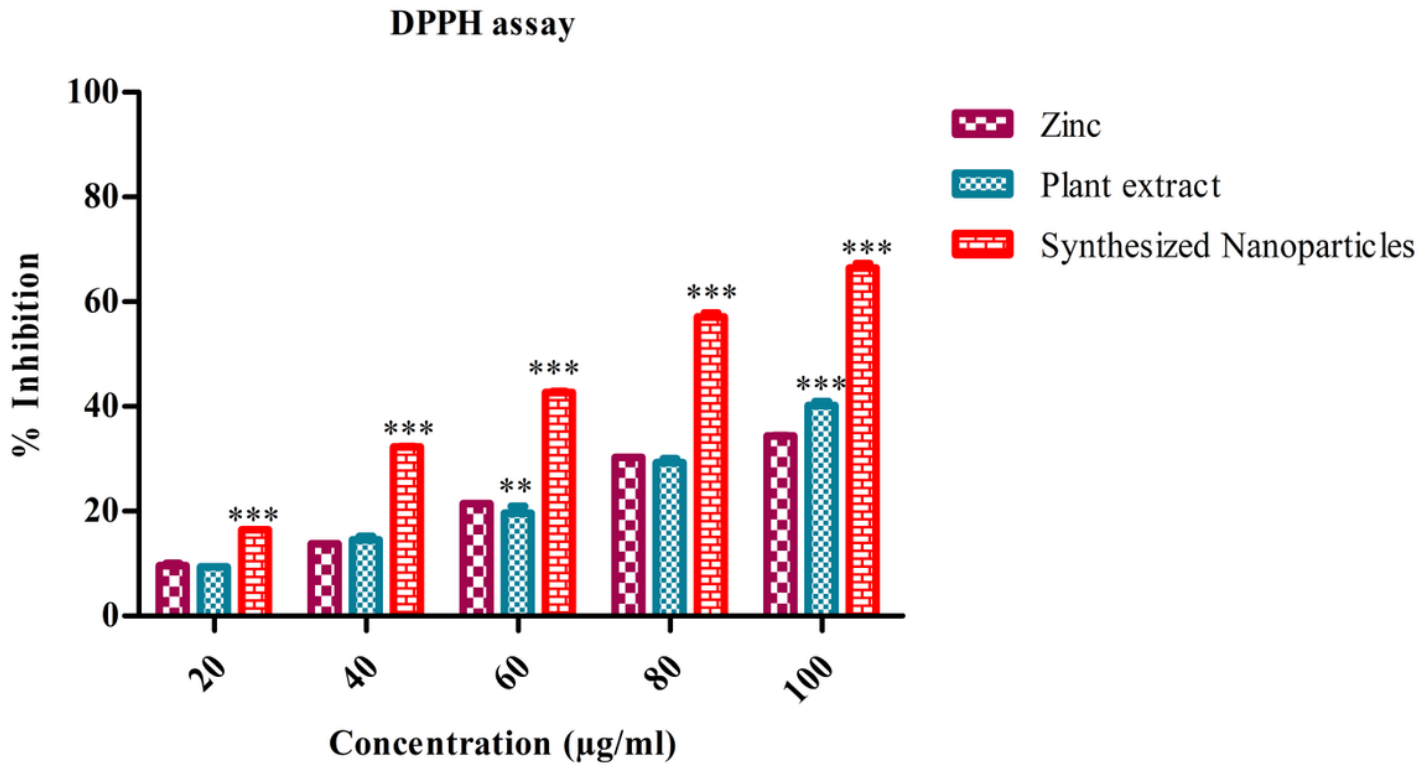

Figure 4

Antioxidant activity; DPPH assay of ZnNPs, plant extract and synthesized NPs at different concentrations (20, 40, 60, 80, 100 µg/mL). The values are expressed as mean ± SD and analyzed by Two-way analysis of variance (ANOVA).

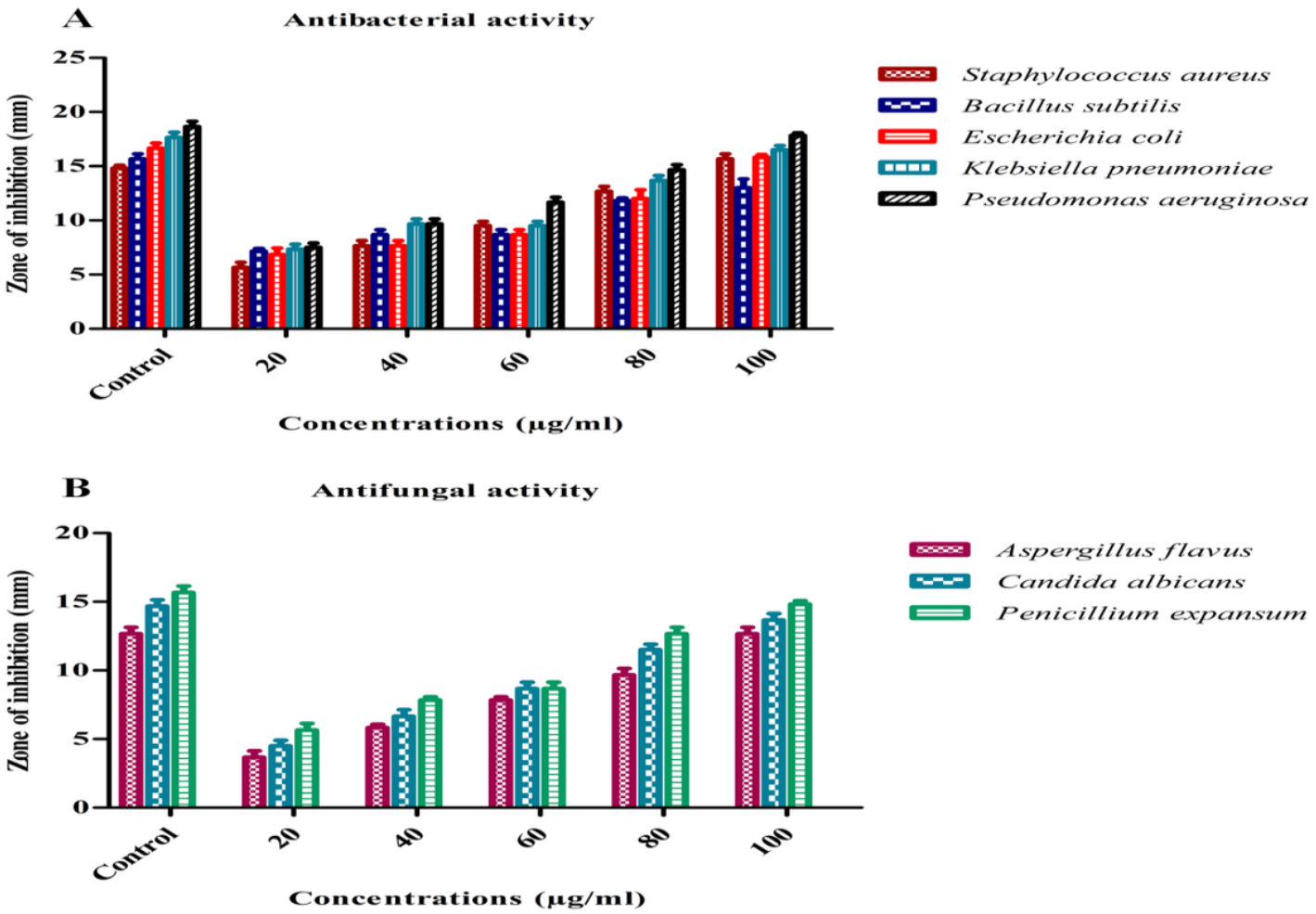

Figure 5

Antibacterial (A) and antifungal (B) activity of ZnNPs on different pathogenic bacteria (E.coli, S. aureus, and P. aeruginosa, B. subtilis, S.typhi and K. pneumonia) at different concentrations (20, 40, 60, 80 and 100 µg/mL) were observed. The control antibiotics were tetracycline (A), fluconazole (B) used for analysis. The zone of inhibition values are expressed as mean ± SD and analyzed by Two-way analysis of variance (ANOVA).

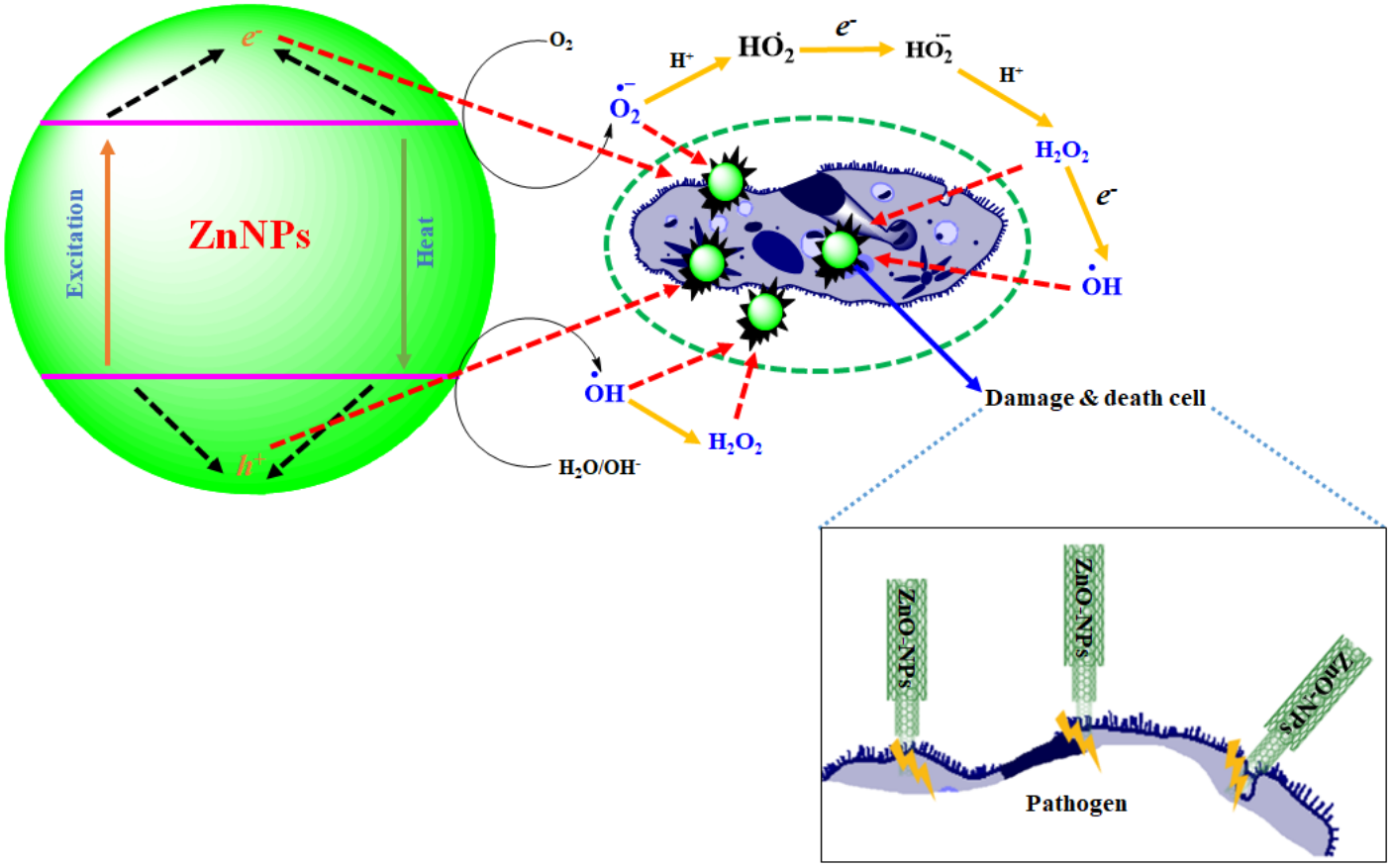

Figure 6

Schematic reason for mechanism of microbes cell damage by ZnO-NPs.

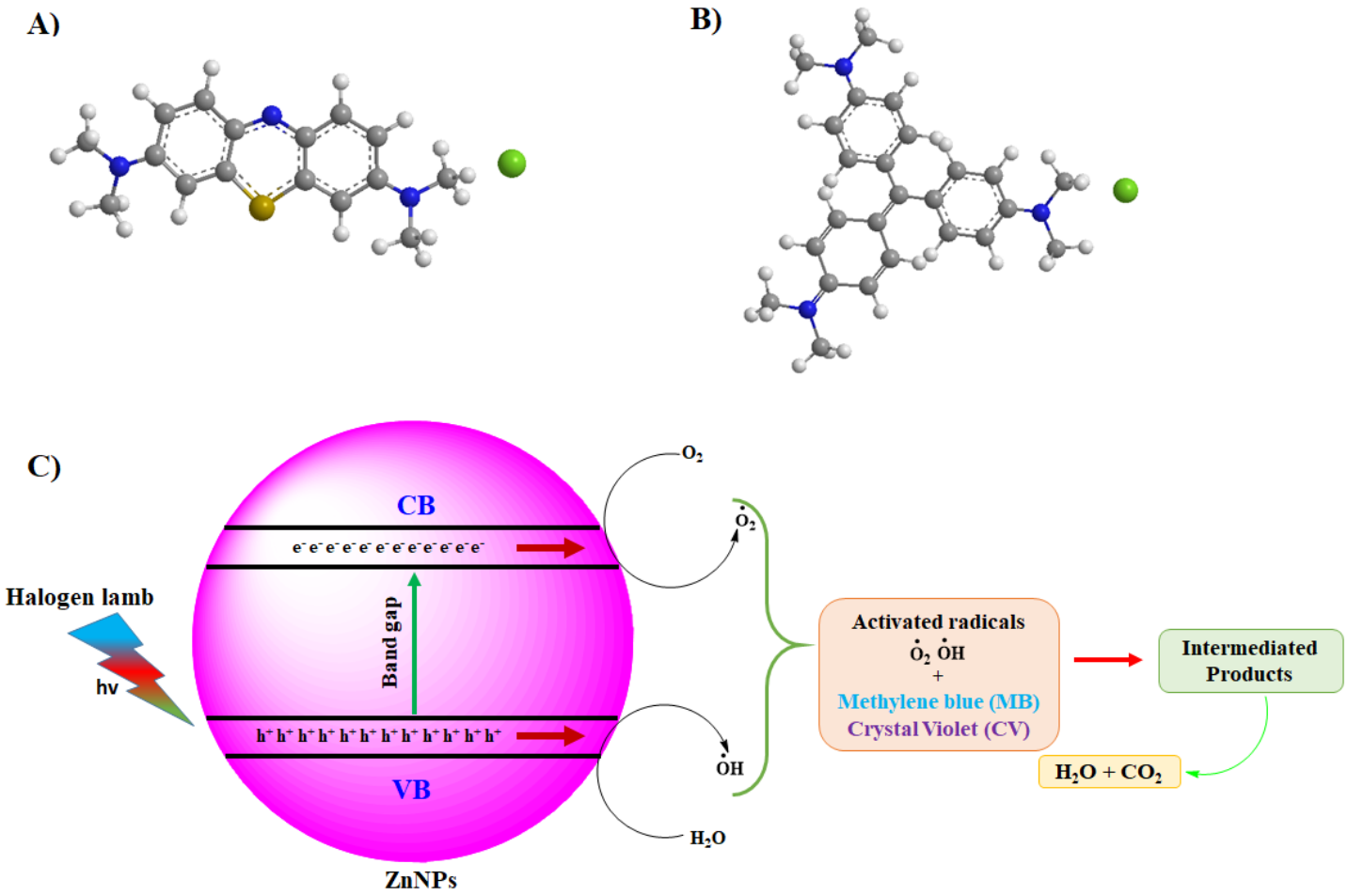

Figure 7

(A) Structure of MB, (B) Structure of CV and (C) Scheme of the photocatalytic mechanism of the biogenic synthesized ZnO-NPs under halogen light irradiation.

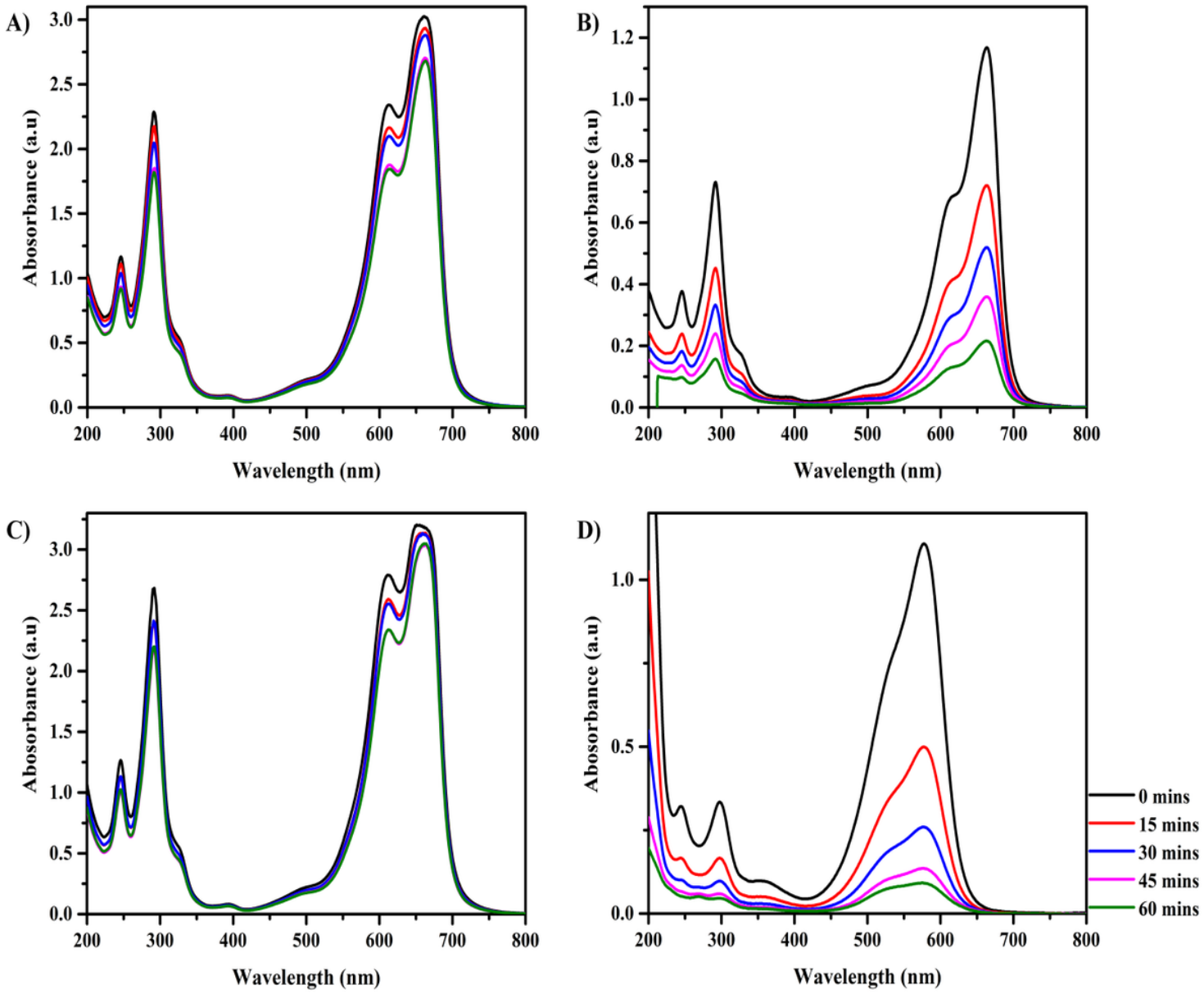

Figure 8

(a) Adsorption spectrum of methylene blue under light irritation (b) adsorption spectrum of ZnO-NPs against methylene blue under light irritation (c) adsorption spectrum of crystal violet under light irritation (d) adsorption spectrum of ZnO-NPs against crystal violet under light irritation.

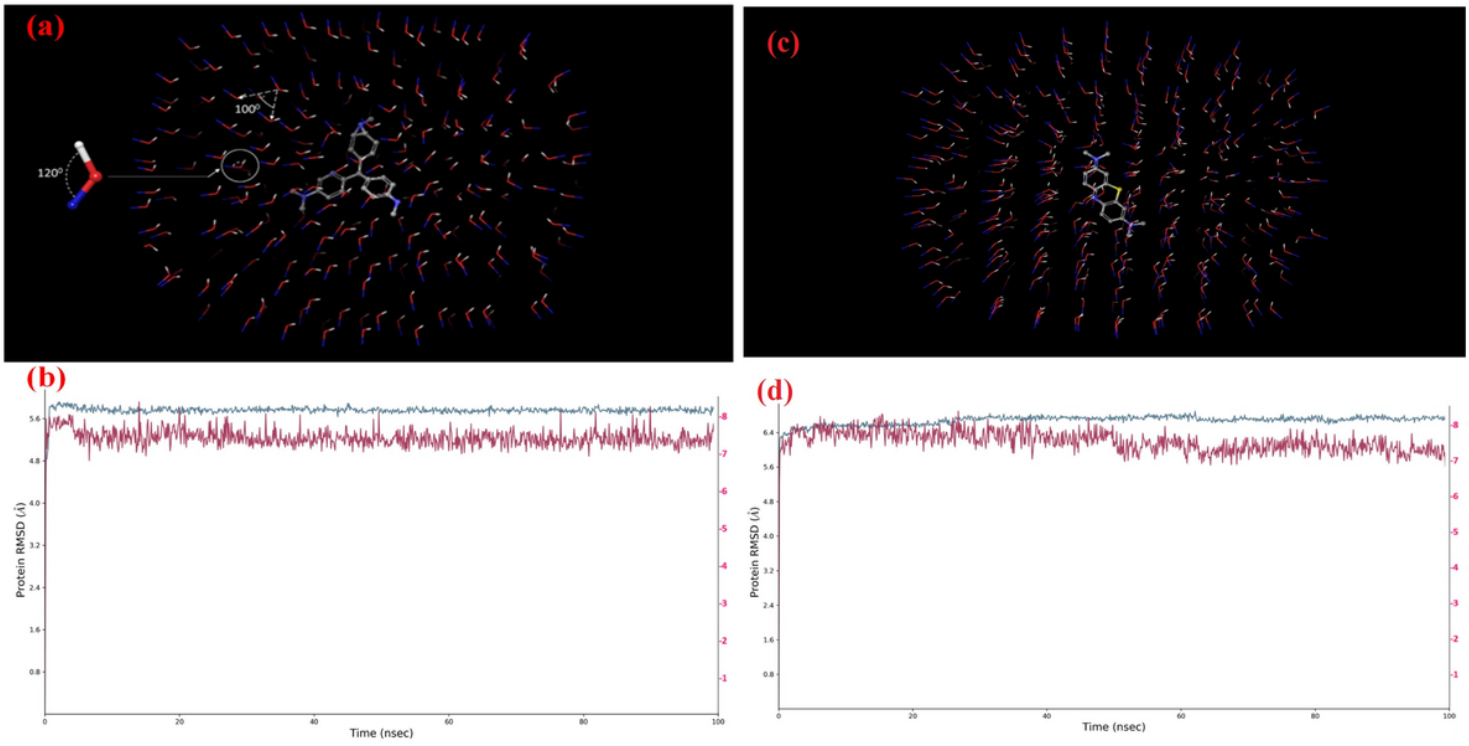

Figure 9

(A) ZnO-NPs–Crystal violet complex scattered projections in the environment with equal geometrical distributions (100º) of the proposed quantity and geometry of the individual structure (120º). (B) Root mean square deviation of ZnONPs layer and crystal violet complex for 100 nano second. (C) ZnO-NPs–Methylene Blue complex scattered projections in the environment with equal geometrical distributions (100º) of the proposed quantity and geometry of the individual structure (120º). (D) Root mean square deviation of ZnO-NPs layer and methylene blue complex for 100 nano second.

Supplementary Files

This is a list of supplementary files associated with this preprint. Click to download.

- GrapicalAbstracts.png